

See discussions, stats, and author profiles for this publication at: <https://www.researchgate.net/publication/331087579>

# Numerical Analysis of Flow Characteristics around a Single-bladed Darrieus Wind Turbine

Conference Paper · January 2018

CITATIONS

0

READS

20

3 authors, including:



**Md. Tanvir Khan**

Khulna University of Engineering and Technology

4 PUBLICATIONS 0 CITATIONS

SEE PROFILE



**Abdullah Al-Faruk**

Khulna University of Engineering and Technology

6 PUBLICATIONS 3 CITATIONS

SEE PROFILE

Some of the authors of this publication are also working on these related projects:



Single-Bladed Darrieus Turbine [View project](#)



A Developed Length Based Product Separating Conveyor for Industrial Automation [View project](#)

# Numerical Analysis of Flow Characteristics around a Single-bladed Darrieus Wind Turbine

Md. Tanvir Khan<sup>1</sup>, Mohammad Ilias Inam<sup>1</sup>, Abdullah Al-Faruk<sup>1</sup>

<sup>1</sup> Department of Mechanical Engineering, Khulna University of Engineering & Technology, Khulna-9203, BANGLADESH

\*tanvir.anik2196@gmail.com

**Abstract—** Renewable energy has no alternative for meeting the world's energy demand due to the increasing price of carbon derivative fuels multiplied by the depletion of fossil fuels in recent years. Wind energy has been identified as one of the most realizable sources of renewable energy industry. Moreover, the wind energy is green, clean and has no harmful effect on the environment. Darrieus wind turbine appears to be promising for the condition of low wind speed though it has a low efficiency compared to the horizontal axis turbines. Moreover, it needs small space for installation, making it suitable for using on the rooftop of urban houses. The objective of this paper is to investigate numerically the characteristics of the developed flow around a single bladed Darrieus wind turbine. The blade is designed using the NACA 0015 profile and is operated at 5 m/s wind velocity. 2D simulations were performed using ANSYS Fluent 16.2, employing the realizable  $k$ -epsilon turbulence model. The numerical model was verified through the independent studies of domain size, mesh size and temporal size. The CFD results under the dynamic cases were presented and the resulting aerodynamic forces were evaluated. The turbine was observed to generate both positive and negative power at certain azimuthal angles at wind velocity 5 m/s. The pressure contours, velocity profiles and the velocity streamlines were drawn which showed different types of vortices around the blade. Result show that, Force and power varies periodically with the azimuthal angles. The calculated average power and power coefficient were found positive after the turbine has come to steady state condition.

**Index Terms—** Darrieus wind turbine, pressure coefficient, vortex, dynamic stall.

## I. INTRODUCTION

Recent instabilities of world economy, due to the increasing price of carbon-derivative fuels along with connected socio-political turbulences, have aroused the interest in the production of renewable energy among the most industrialized western nations. In this scenario, the continuous quest for clean energy is now focusing on the local production of electric power, spread in a wide area, so as to cooperate with the big electric power plants located in just few specific strategic locations of the countries. One of the most promising resources is the Eolic energy source associated with local production of clean electric power inside built environment such as industrial and residential areas [1]. Nowadays, interests in two types of modern wind turbines, namely, horizontal-axis (HAWTs) and vertical-axis (VAWTs) wind turbines, are continuously growing [2]. Despite lower efficiency Vertical axis wind turbines (VAWTs), provide several advantages including lower cost, necessity of less maintenance, lower sound emission, independence from wind directions due to rotor axial symmetry, better wind impact on blade and so on, if compared with the classical horizontal-axis wind turbines (HAWTs) [3]. Another salutary influence is that VAWTs are Omni-directional, accepting wind from any

direction without any yawing mechanism [4]. In brief, it has a number of promising features which if exploited properly can make it a better alternative to fulfil the world's energy demand. Although currently large scale VAWTs are not economically attractive, they offer energy solutions for the remote places away from the main distribution lines and places where large wind farms cannot be installed for environmental concerns and small-scale dispersed generation units are preferred [5]. That is why mass production of VAWTs has recently been started as small scale wind power generating units [6].

Two types of modern VAWTs, namely, Savonius (SWT) and Darrieus (DWT) wind turbine are available. Among them DWT is more suitable for power production for its high rotating speed. Moreover, it increasingly appreciated and often considered as the most promising solution in the built environment, due to very low noise levels and reduced sensitivity to the turbulent oncoming wind [7-9]. In addition, recent studies [8,10] put in evidence that some benefits in terms of power increase can be obtained from a Darrieus functioning under skewed flow, mainly connected to the possibility of exploiting an increased swept area (projected perpendicularly to the mainstream direction). Darrieus is a lift type wind turbine of which the blades are of airfoil shaped. A vast amount of research has been done on DWTs and still continuing. A blade element momentum single stream tube numerical model was first developed by Templin [11] to predict the performance of a VAWT. KIRKE [12] proposed that high solidity was able to improve the self-starting torque but with lower peak power coefficient and narrower operating range. Moreover, a blade element momentum multiple stream tube numerical model was developed by Strickland [13,14] for predicting the performance of a VAWT rotor. Furthermore, DOMINY et al [15] indicated that three-bladed wind turbine had the potential to self-start but the self-starting of two-bladed rotor was dependent on its initial starting orientation. In addition, both HILL et al [16] and ISLAM et al [17] pointed out that cambered section would produce a higher tangential force and more energy per revolution than symmetrical section, hence asymmetric airfoils with high-lift and low-drag were much suitable and desirable airfoils for better self-starting and power coefficient. Analytical and numerical aerodynamic models were presented to investigate the performance of VAWT by Paraschivoiu [18–21], focusing on the phenomenon of dynamic stall. However, though researchers argued for use of greater thickness airfoils to enhance self-starting capability [17], KIRKE [12] and WANG et al [22] claimed that increasing section thickness seems to make slightly contribution to aerodynamic performance improvement at low tip speed ratios. Mertens [23] developed a blade element-momentum multiple stream tube model to

predict the performances of a fast rotating VAWT in the skewed flow on a roof.

Bangladesh, as an underdeveloped country, can achieve huge benefits by properly utilizing the wind power. Wind turbine can be used in those remote places where electricity has yet not been reached. Though the wind speed of Bangladesh is not so high, however, DWT can easily be operated by the available wind speed. The annual wind speed of some places is listed in table 1 from which it is observed that the average speed varies from 2-5 m/s, which is high enough to operate DWT. This paper aims to investigate the flow development of a single-bladed DWT using Computational Fluid Dynamics (CFD) methods. The blade was constructed of NACA 0015 profile and was operating at 5 m/s wind velocity and 0.1 tip speed ratio. Two dimensional simulations were performed using a commercial CFD package, ANSYS Fluent 16.2, employing the Realizable K-epsilon turbulence model [24] with scalable wall function. The CFD results from the dynamic case were presented and the resulting aerodynamic forces were evaluated. Moreover, the Power coefficients for 5 m/s wind velocity were calculated.

TABLE I  
ANNUAL WIND VELOCITIES OF DIFFERENT ZONES IN BANGLADESH [25]

Stations	Annual wind speed (m/s)	Stations	Annual wind speed (m/s)
Dhaka	2.45	Khulna	2.38
Chittagong	5.37	Cox's Bazar	4.48
Sylhet	2.42	Raj Shahi	2.46
Jessore	3.42	Rangpur	2.22

## II. NUMERICAL MODEL DEVELOPMENT

ANSYS FLUENT provides the opportunity to solve both steady state and transient flow analyses with a variety of turbulence modelling. Continuity equation and Navier Stokes equation are solved in all computational fluid dynamics (CFD) analysis, and in compressive flow or heat transfer cases. A numerical model was developed for this simulation, where the governing equations were employed to describe the flow over the turbine. Continuity and momentum equations were included in the models the model as the model neglects heat transfer.

Continuity equation:

$$\frac{\partial(\rho v_x)}{\partial x} + \frac{\partial(\rho v_y)}{\partial y} + \frac{\partial(\rho v_z)}{\partial z} + \frac{\partial \rho}{\partial t} = 0$$

Where,  $v_x$ ,  $v_y$  and  $v_z$  are the fluid velocities in the  $x$ ,  $y$ , and  $z$  directions, respectively, and  $\rho$  is the density of the fluid. The equation states that the time rate at which mass increases within the control volume is equal to the net influx of mass across the control surface.

Navier Stokes Equation:

$$\frac{\partial \rho u}{\partial t} + \nabla \cdot (\rho u u) = \nabla \cdot \mu \nabla u - \frac{\partial \rho}{\partial x} + \rho g_x$$

$$\text{X-momentum: } u \frac{\partial u}{\partial x} + v \frac{\partial u}{\partial y} = -\frac{\partial \rho}{\partial x} + \frac{1}{\text{Re}} \left[ \frac{\partial \tau_{xx}}{\partial x} + \frac{\partial \tau_{xy}}{\partial y} \right]$$

$$\text{Y-momentum: } u \frac{\partial v}{\partial x} + v \frac{\partial v}{\partial y} = -\frac{\partial \rho}{\partial y} + \frac{1}{\text{Re}} \left[ \frac{\partial \tau_{xy}}{\partial x} + \frac{\partial \tau_{yy}}{\partial y} \right]$$

Realizable k-epsilon model:

Realizable  $k$ - $\epsilon$  turbulence was used for rotating zones which benefits include strong pressure gradient, flow separation and performance improvement in the flow recirculation [24].

Transport equations:

$$\frac{\partial}{\partial t}(\rho \kappa) + \frac{\partial}{\partial x_j}(\rho \kappa u_j) = \frac{\partial}{\partial x_j} \left[ \left( \mu + \frac{\mu_t}{\sigma_\kappa} \right) \frac{\partial \kappa}{\partial x_j} \right] + G_\kappa + G_b - \rho \epsilon - Y_M + S_\kappa$$

$$\text{And } \frac{\partial}{\partial t}(\rho \epsilon) + \frac{\partial}{\partial x_j}(\rho \epsilon u_j) = \frac{\partial}{\partial x_j} \left[ \left( \mu + \frac{\mu_t}{\sigma_\epsilon} \right) \frac{\partial \epsilon}{\partial x_j} \right] + \rho C_1 S_\epsilon - \rho C_2 \frac{\epsilon^2}{k + \sqrt{\nu \epsilon}} + C_{1\epsilon} \frac{\epsilon}{k} C_3 G_b + S_\epsilon$$

$$\text{Where, } C_1 = \max \left[ 0.43 \frac{\eta}{\eta + 5} \right], \eta = S \frac{k}{\epsilon}, S = \sqrt{2 S_{ij} S_{ij}} \quad [26]$$

## III. COMPUTATIONAL SET UP

The computational domain was constructed of two different zones, namely, stationary zone and rotating zone including the turbine blade [2]. The rotating zone was generated bi-directionally from the blade surface resulting in an annulus shaped zone, that rotated at a predefined angular velocity as shown in Fig. 1. The square shaped domain dimension is 50C by 50C, based on chord length (C) and the centre of the rotating zone was placed at the middle of the square, which was also chosen by Mohamed [24]. Before finalize the domain, different domain sizes were taken and the domain independence test was done.

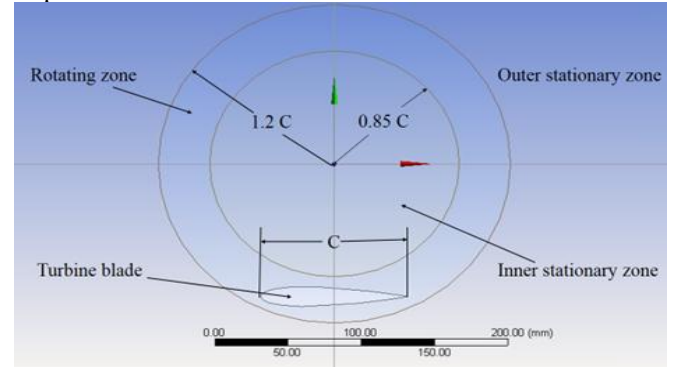


Fig. 1 The computational domain of the numerical analysis

Different sizes of unstructured mesh were employed in this analysis, combining element size of 0.003 mm near the blade for precisely analysing the flow characteristics and 0.008 mm further from the blade. 20 inflation layers were used with 5 mm thickness in the vicinity of the blade surface to better resolve the boundary layer as illustrated in Fig. 2.

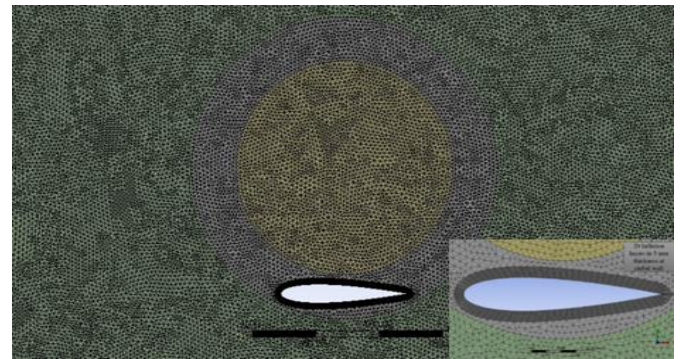


Fig. 2 The computational grid used in the simulation

The selected node and element numbers were 1232362 and 2459030, respectively, after executing grid independence test. The combined grid was chosen instead of single grid to reduce the complexity of the mesh generation. The similar technique

was employed in the literature [2, 27, 28] and good agreements with the measurements were shown. The stationary and rotating zones were linked via the sliding interface boundary condition. Velocity inlet and pressure outlet boundary conditions were used at the upstream and downstream section, respectively, and symmetry condition was used at the other two sides to reduce the computational effort as done by Castelli [29, 30]. The blade was placed in the rotating zone that can rotate with the rotating zone of the same angular velocity between the stationary zones. No slip wall is set as the boundary condition on the blade surface. To capture the flow phenomena around the blade precisely, as minimal as 0.005-time step size was used after time independence verification. The turbine blade was set with an initial clockwise rotation and the air was allowed to flow around the turbine blade at a known velocity (2.5 m/s). Due to wind velocity, a net torque was developed for the combined effect of the air kinetic energy and the blade rotation. The normal and tangential force as well as the power had been calculated from the developed lift and drag force on the blade at each azimuthal position. Realizable  $k-\varepsilon$  turbulence model, referred by Mohammed [24], was used for rotating zones. Simple pressure-based solver was selected along with second order implicit transient formulation. All solution variables were solved via the second order upwind discretization scheme that is also followed by Bangga [2]. Scalable wall function was used and  $Y^+ \geq 11.126$  was ensured for the analysis.

#### IV. CFD RESULT

The simulations were carried out for 10 blade revolutions and the last three revolutions were extracted and averaged which is also done by Bangga [2]. Flow characteristics around the blade are observed and different types of vortex, generated for dynamic stall and the blade vortex interaction, are analysed. The tangential ( $F_T$ ) force and normal ( $F_N$ ) force for different tip speed ratios had been calculated from the simulation data.

##### A. Flow Field Analysis of Darrieus Wind Turbine

Flow characteristics such as pressure coefficient contour, velocity contour and streamline has been determined after every  $30^\circ$  interval of azimuthal angle ( $\theta$ ) in the analysis. Pressure coefficient is a dimensionless number that describes the relative pressure throughout a flow field and is defined by,  $C_p = \frac{P - P_\infty}{1/2 \rho_\infty V_\infty^2}$ . It is a vital factor for wind turbine aerodynamics which causes a significant change in the lift and drag as well as the power generation.

At the initial stage of the turbine rotation when the blade is at  $\theta = 0^\circ$ , air strikes at the leading edge of the blade which is the stagnation point of maximum pressure as shown in Fig. 3(a). As the blade is shaped as a symmetrical airfoil, no pressure variation occurs at the upper and lower surface of the blade, consequently, no lift is generated as evident from Fig. 3(a). Lower velocity occurs at the lower surface of the blade near the trailing edge as shown in Fig. 4(a). With the increment of azimuthal angle ( $\theta$ ), the angle of attack ( $\alpha$ ) also increase, consequently, flow separation occurs at the upper surface of the blade (Fig. 5(a)). The more the angle of attack ( $\alpha$ ) increase the more separation, starts near the leading edge and stall phenomena occurs. Flow separates from the leading edge at  $\theta = 30^\circ$  where the maximum velocity occurs as shown in Fig. 4(b). A vortex (TEV) is visible at the trailing

edge as observed in Fig. 5(b). Pressure at the upper surface is lower than the lower surface and maximum pressure occurs at the lower surface near the leading edge as shown in Fig. 3(b). However, higher pressure occurs near the leading edge of the blade and lower pressure occur at the trailing edge of the blade due to the formation of vortices TEV (Fig. 3(c)), when the blade comes to  $\theta = 60^\circ$ . Flow separation occurs from both the leading and the trailing edge due to the dynamic stall (DS) as illustrated in Fig. 5(c). Higher velocity occurs near the trailing edge as shown in Fig. 4(c).

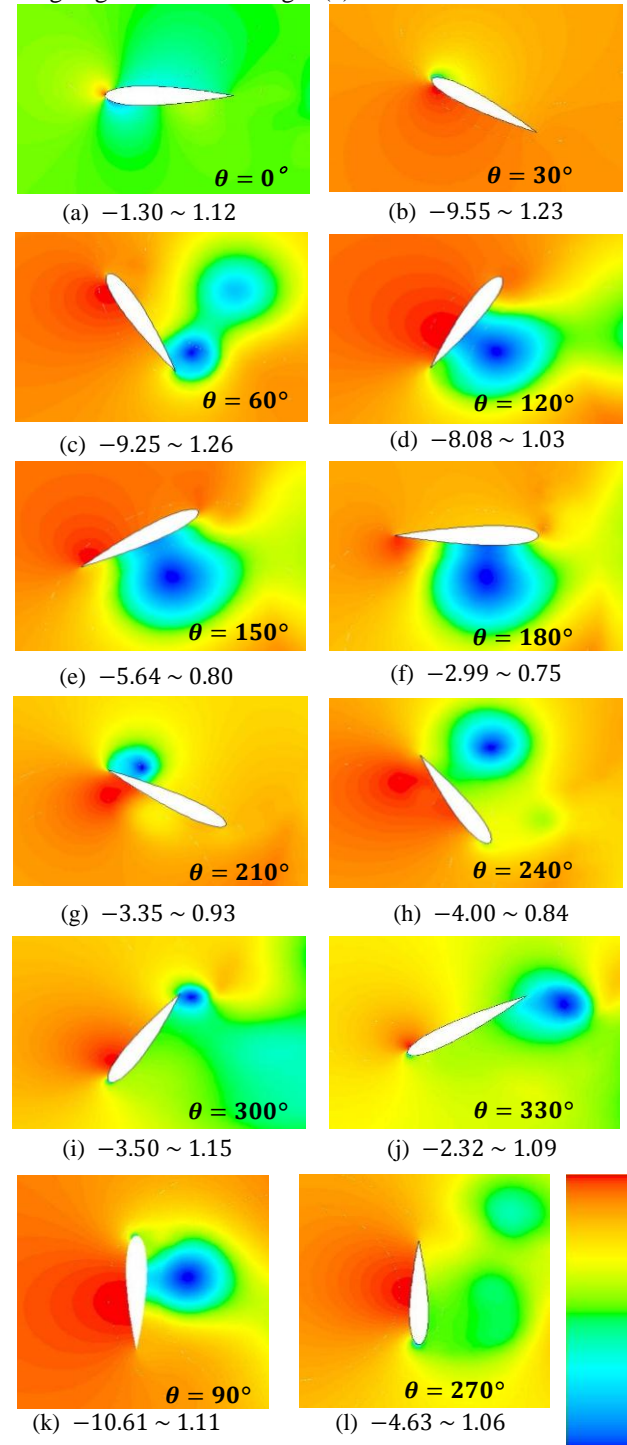


Fig. 3 Contour of pressure coefficient with different azimuthal angle  $\theta$  at 5 m/s wind velocity. The minimum and maximum values of the colour legend are mentioned below the figure.

Lower pressure occurs at the downstream of the blade at  $\theta = 90^\circ$  position of blade as shown in Fig. 3(k). Both

clockwise and anti-clockwise LEV is formed as shown in Fig. 5(k). Moreover, Higher velocity region is visible at the downstream of the blade as illustrated in Fig. 4(k). Velocity at the leeward side is very low. The leading-edge vortex departed from the blade when the blade pass  $\theta = 90^\circ$  and formation of anticlockwise TEV starts.

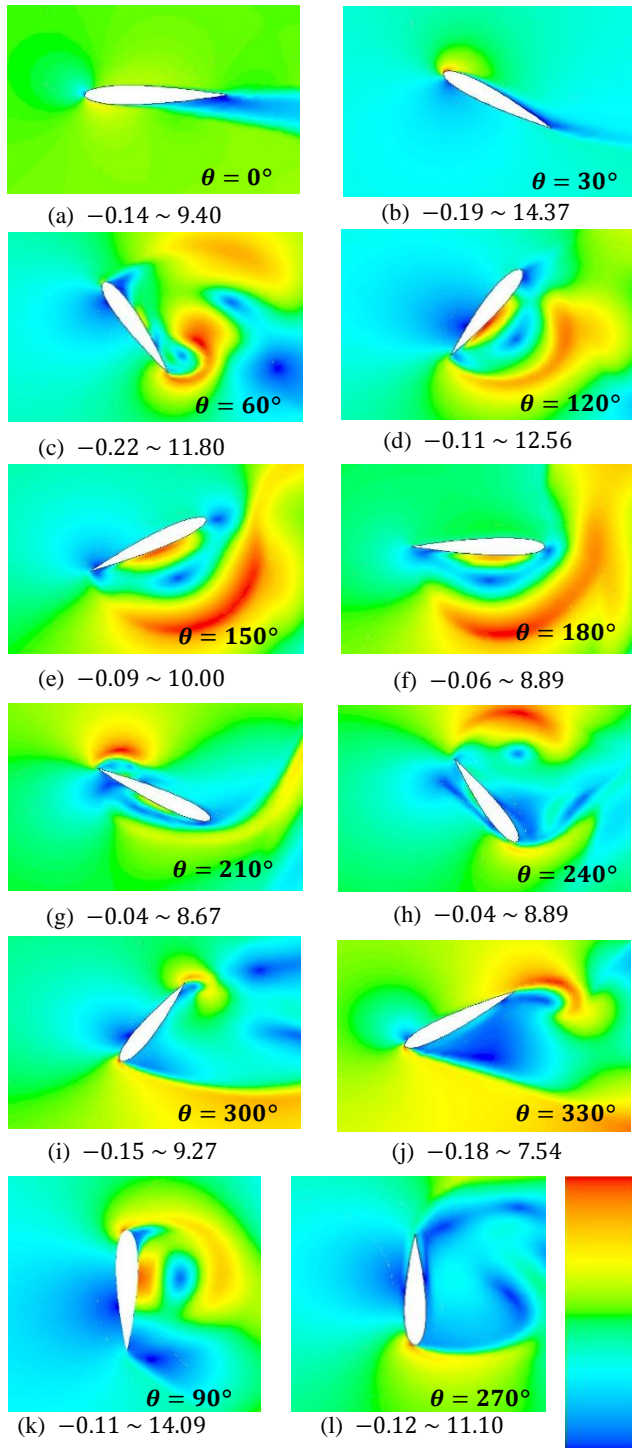


Fig. 4 Contour of velocity profile with different azimuthal angle  $\theta$  at 5 m/s wind velocity. The minimum and maximum values of the colour legend are mentioned below the figure.

Flow characteristics at  $\theta = 120^\circ, 150^\circ, 180^\circ$  are almost similar. Lower pressure occurs near the middle of the blade at the downstream zone where the anticlockwise vortex is formed as shown in Fig. 4(d, e, f), respectively. Velocity at the downstream is higher than the upstream zone according to the Bernoulli's equation (Fig. 4(d, e, f)).

Flow separates from both the leading and the trailing edge of the blade (Fig. 4(d, e, f)). However, Maximum pressure occurs at the upstream of the trailing edge at  $\theta = 210^\circ$  where the velocity is minimum Fig. 3(g). Clockwise TEV is visible at the upper surface of the blade for which the pressure is minimum and velocity is higher Fig. 4(g). Furthermore, other two vortices are visible at the upstream of the blade due to dynamic stall as shown in Fig. 5(g).

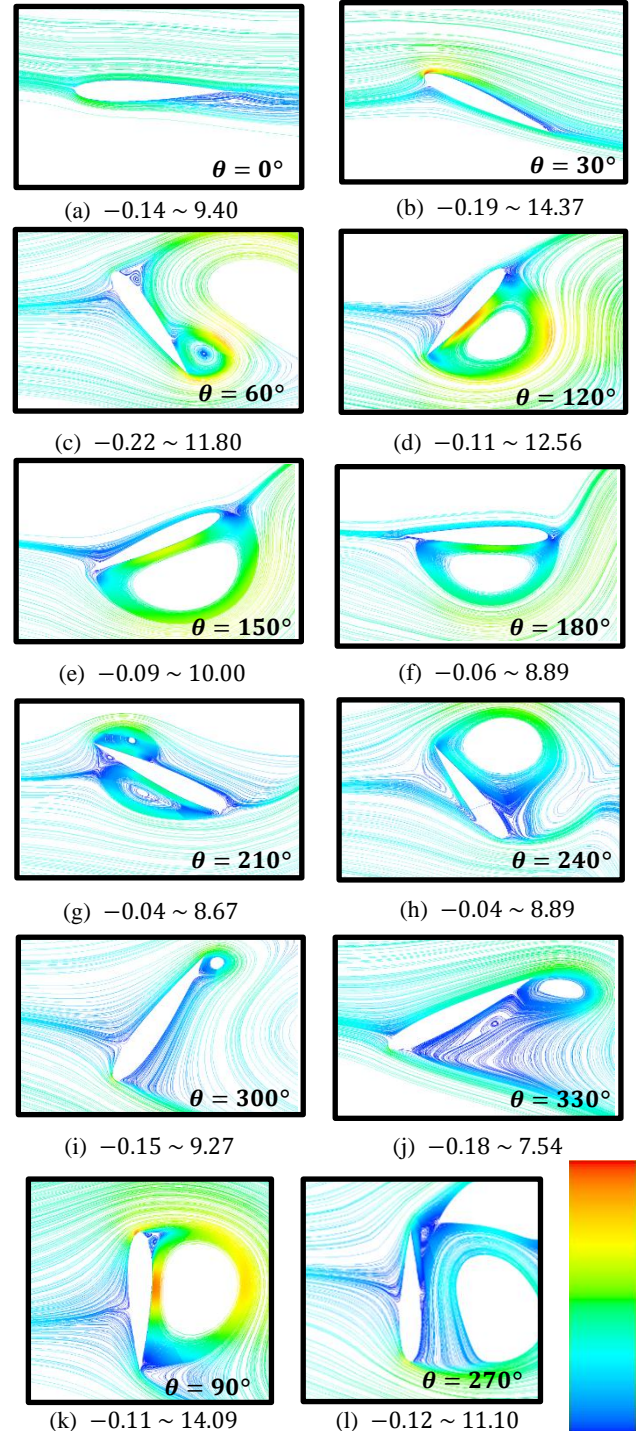


Fig. 5 Contour of stream line with different azimuthal angle  $\theta$  at 5 m/s wind velocity. The minimum and maximum values of the colour legend are mentioned below the figure.

The lower pressure occurs near the trailing edge at  $\theta = 240^\circ$  as shown in Fig. 3(h). The previously formed TEV has the tendency to detach from the blade as illustrated in Fig. 5(h). Moreover, velocity at the blade downstream is minimum

(Fig. 4(h)). Reattachment of flow occur near the leading edge of the blade. In the presence of laminar-turbulent transition, flow may reattach in such a way that, initially laminar boundary flow may separate because of an adverse pressure gradient. Then the flow becomes strongly unstable and hence turbulent. Hence, it reattaches further downstream because of the stronger resistance of turbulent boundary-layer flow against separation. After the cycle complete the flow phenomena repeats as the turbine come to a steady state. Anticlockwise vortex forms at the leading edge and clockwise vortex forms at the trailing edge of the blade at  $\theta = 270^\circ$  as shown in Fig. 5(i). Flow separates from the trailing edge and higher velocity is shown near the trailing edge (Fig. 4(l)). Maximum pressure occurs at the upstream of the blade (Fig. 3(l)). At  $\theta = 300^\circ$  and  $330^\circ$  low pressure occurs at the trailing edge of the blade as shown in Fig. 3(i, j), respectively. Flow separation occurs both from the leading edge and the trailing edge and a clockwise TEV is vortex is visible Fig. 5(i, j). Another anticlockwise vortex is visible at the middle of blade at  $\theta = 330^\circ$  (Fig. 5(j)). Velocity is maximum at the leading edge and the trailing edge as shown in Fig. 4(i, j), respectively. Flow characteristics are the same as  $\theta = 0^\circ$  when  $\theta = 360^\circ$ .

### B. Tangential ( $F_T$ ) and Normal ( $F_N$ ) Force

The tangential and normal forces vary periodically with the azimuthal angle after the 7<sup>th</sup> revolution of the rotor blade in the simulation. To determine tangential and normal forces, lift and drag forces are calculated from the lift ( $C_L$ ) and drag ( $C_D$ ) coefficients and then the tangential and normal forces are calculated from the lift and drag forces. At the beginning of the turbine rotation, both the forces are positive. When the blade comes to  $\theta = 45^\circ$  azimuthal position, lower pressure occurs at the upper surface of the blade and the direction of  $F_T$  changes along with the change of lift ( $C_L$ ) and drag ( $C_D$ ) coefficients as illustrated in Fig. 6. After the separation of the lower pressure zone from the upper surface,  $F_T$  tends to increase at  $\theta = 60^\circ$  until lower pressure occurs at the upper surface of the blade again as a consequence of DS.  $F_T$  decreases gradually at  $\theta = 90^\circ$  for the occurrence of lower pressure at the downstream and high-pressure drag at the blade upstream. At the blade's position of  $\theta = 120^\circ$ , lower pressure zone detached from the upper surface, therefore, the force tends to increase. When  $\theta = 150^\circ$  different types of vortex form around the blade and as a result of blade vortex interaction,  $F_T$  decrease to  $\theta = 210^\circ$ . After  $\theta = 210^\circ$  when the lower pressure zone tends to come to the middle of the blade  $F_T$  increase and when lower pressure zone separates at  $\theta = 240^\circ$  the force tends to decrease. At  $\theta = 270^\circ$  force increase as higher pressure occurs at the upstream zone. Again, lower pressure occurs at the trailing edge of the blade at  $\theta = 300^\circ$  and the force increase. So, it can be decided for the second half of the blade rotation when the lower pressure occurs at the trailing edge, the tangential force tends to increase. Also, for the first half cycle, the force is positive and for the last half cycle, the force is negative as shown in Fig. 6.

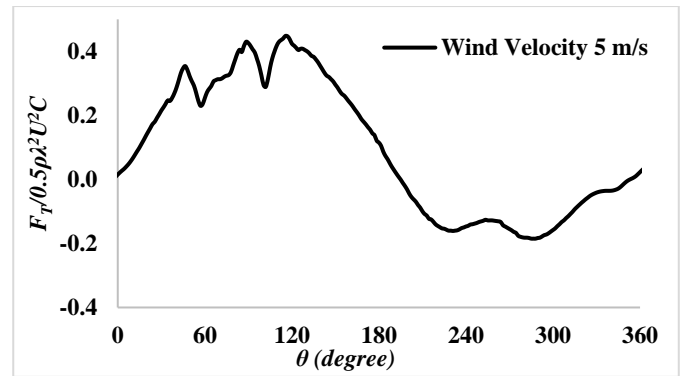


Fig. 6 Variation of non-dimensional tangential force with the azimuthal angle for wind velocity 5 m/s

The normal force changes dramatically around the blade surface due to dynamic stall and the pressure variation around the blade as shown in Fig. 7.  $F_N$  increase gradually till the blade comes to  $\theta = 45^\circ$ , then it tends to decrease up to  $\theta = 135^\circ$ , and again the force increases until  $\theta = 180^\circ$  and at this position no force acts around the blade. After that  $F_N$  decrease to  $\theta = 225^\circ$  and then again increase up to  $\theta = 315^\circ$ . Finally, the force decreases for the rest of the cycle and then repeats as shown in Fig. 7. It is observed that from  $\theta = 90^\circ$  to  $\theta = 270^\circ$  the net force is negative and for other positions the force is positive.

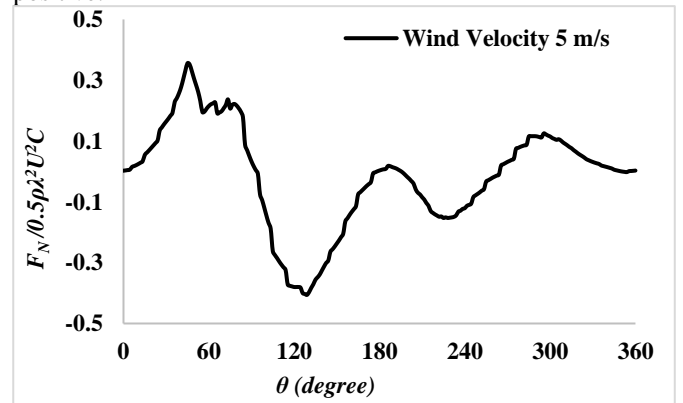


Fig. 7 Variation of non-dimensional normal force with the azimuthal angle for wind velocity 5 m/s

### C. Power Coefficient

Power coefficient is the ratio of the generated output power ( $P$ ) to the theoretical input power ( $P_{in}$ ). As the turbine rotates clockwise direction the negative tangential force ( $F_T$ ) generate the positive power which can be defined by,  $P = -\omega R F_t$  [2]. The theoretical input power is  $P_{in} = \frac{1}{2} \rho A V^3$ , where  $A$  is the swept area,  $V$  is the air velocity and  $\rho$  is air density. For wind velocity 5 m/s the calculated average power coefficient is 0.056 which is calculated after the turbine comes to a steady state condition. It is observed that the power coefficient is proportional to the rotor radius. So, the more the radius of the rotor the more the power coefficient will be and the turbine will generate more power.

## V. CONCLUSIONS

Computational fluid dynamics simulations have been carried out to study a single bladed Darrieus wind turbine under the dynamic stalled condition at wind velocity 5 m/s. The studied turbine blade was constructed of NACA 0015 airfoil profile. The flow characteristics around the bladed

surface were investigated and highlighted as the main focus of the paper. The tangential and the normal force and the average power coefficient had been calculated. It is observed that different types of vortex are generated around the blade surface as a consequence of dynamic stall. Moreover, pressure varies considerably at the different position of the blade which affect the tangential forces around the blade. Power generation, as well as the tangential force, varies positively and negatively with the azimuthal angle. The average power coefficient at the steady state is positive which indicate that the turbine can produce net positive power.

## REFERENCES

- [1] Batista, N. C., Melício, R., Mendes, V. M., Figueiredo, J., & Reis, A. H. (2013, April). Darrieus Wind Turbine Performance Prediction: Computational Modeling. In *Doctoral Conference on Computing, Electrical and Industrial Systems* (pp. 382-391). Springer, Berlin, Heidelberg.
- [2] Bangsa, G., Hutomo, G., Wiranegara, R., & Sasongko, H. (2017). Numerical study on a single bladed vertical axis wind turbine under dynamic stall. *Journal of Mechanical Science and Technology*, 31(1), 261-267.
- [3] Castelli, M. R., & Benini, E. (2012). Effect of blade inclination angle on a Darrieus wind turbine. *Journal of turbomachinery*, 134(3), 031016.
- [4] Chaichana, T., & Chaitep, S. (2010). Wind power potential and characteristic analysis of Chiang Mai, Thailand. *Journal of mechanical science and technology*, 24(7), 1475-1479.
- [5] Bishop, J. D., & Amaratunga, G. A. (2008). Evaluation of small wind turbines in distributed arrangement as sustainable wind energy option for Barbados. *Energy Conversion and Management*, 49(6), 1652-1661.
- [6] Islam, M., Fartaj, A., & Ting, D. S. K. (2004). Current utilization and future prospects of emerging renewable energy applications in Canada. *Renewable and Sustainable Energy Reviews*, 8(6), 493-519.
- [7] Balduzzi, F., Bianchini, A., Carnevale, E. A., Chesi, A., & Ferrari, L. (2010, September). Influence of the building geometry on microeolic installations in the urban context. In *Proc. of World Renewable Energy Congress XI*.
- [8] Mertens, S., van Kuik, G., & van Bussel, G. (2003). Performance of an H-Darrieus in the skewed flow on a roof. *Journal of Solar Energy Engineering*, 125(4), 433-440.
- [9] Mertens, S. (2003). The energy yield of roof mounted wind turbines. *Wind engineering*, 27(6), 507-518.
- [10] Ferreira, C., van Kuik, G., & van Bussel, G. (2006). An analytical method to predict the variation in performance of an H-Darrieus in skewed flow and its experimental validation. In *Proceedings of the European Wind Energy Conference 2006*.
- [11] Templin, R. J. (1974). Aerodynamic performance theory for the NRC vertical-axis wind turbine. *NASA STI/Recon Technical Report N, 76*.
- [12] Kirke, B. K. (1998). *Evaluation of self-starting vertical axis wind turbines for stand-alone applications* (Doctoral dissertation, Griffith University).
- [13] Strickland, J. H. (1975). *Darrieus turbine: a performance prediction model using multiple streamtubes* (No. SAND-75-0431). Sandia Labs., Albuquerque, N. Mex.(USA).
- [14] Oler, J. W., Strickland, J. H., Im, B. J., & Graham, G. H. (1983). *Dynamic stall regulation of the Darrieus turbine* (pp. 1-162). Albuquerque, NM: Sandia National Laboratories.
- [15] Dominy, R., Lunt, P., Bickerdyke, A., & Dominy, J. (2007). Self-starting capability of a Darrieus turbine. *Proceedings of the Institution of Mechanical Engineers, Part A: Journal of Power and Energy*, 221(1), 111-120.
- [16] Hill, N., Dominy, R., Ingram, G., & Dominy, J. (2009). Darrieus turbines: the physics of self-starting. *Proceedings of the Institution of Mechanical Engineers, Part A: Journal of Power and Energy*, 223(1), 21-29.
- [17] Islam, M., Ting, D. S., & Fartaj, A. (2007). Desirable airfoil features for smaller-capacity straight-bladed VAWT. *Wind Engineering*, 31(3), 165-196.
- [18] Allet, A., & Paraschivoiu, I. (1995). Viscous flow and dynamic stall effects on vertical-axis wind turbines. *International Journal of Rotating Machinery*, 2(1), 1-14.
- [19] Brahim, M. T., Allet, A., and Paraschivoiu, I., 1995, "Aerodynamic Analysis Models for Vertical-Axis Wind Turbines," Int. J. Rotating Mach., 2, 1, pp 15-21.
- [20] Masson, C., Leclerc, C., & Paraschivoiu, I. (1998). Appropriate dynamic-stall models for performance predictions of VAWTs with NLF blades. *International Journal of Rotating Machinery*, 4(2), 129-139.
- [21] Paraschivoiu, I. (2002). *Wind turbine design: with emphasis on Darrieus concept*. Presses inter Polytechnique.
- [22] Tao, W. Y. C. Z. (2006). Numerical investigation of dynamic stall vortex movement of different-thickness airfoils [J]. *Journal of Beijing University of Aeronautics and Astronautics*, 2, 006.
- [23] Mertens, S., van Kuik, G., & van Bussel, G. (2003, January). Performance of a high Tip Speed Ratio H-Darrieus in the skewed flow on a roof. In *ASME 2003 Wind Energy Symposium* (pp. 136-145). American Society of Mechanical Engineers.
- [24] Mohamed, M. H., Ali, A. M., & Hafiz, A. A. (2015). CFD analysis for H-rotor Darrieus turbine as a low speed wind energy converter. *Engineering Science and Technology, an International Journal*, 18(1), 1-13.
- [25] Bangladesh Meteorological Department
- [26] Fluent, A. N. S. Y. S. (2011). Ansys fluent theory guide. *ANSYS Inc., USA, 15317, 724-746*.
- [27] Qin, N., Howell, R., Durrani, N., Hamada, K., & Smith, T. (2011). Unsteady flow simulation and dynamic stall behaviour of vertical axis wind turbine blades. *Wind Engineering*, 35(4), 511-527.
- [28] Hutomo, G., Bangsa, G., & Sasongko, H. (2016). CFD studies of the dynamic stall characteristics on a rotating airfoil. *Applied Mechanics and Materials*, 836, 109-114.
- [29] Castelli, M. R., Englaro, A., & Benini, E. (2011). The Darrieus wind turbine: Proposal for a new performance prediction model based on CFD. *Energy*, 36(8), 4919-4934.
- [30] Castelli, M. R., Dal Monte, A., Quaresimin, M., & Benini, E. (2013). Numerical evaluation of aerodynamic and inertial contributions to Darrieus wind turbine blade deformation. *Renewable Energy*, 51, 101-112.